Research article

Polyurea/Fused-silica interfacial decohesion induced by impinging tensile stress-waves

Mica Grujicic *, Jennifer S. Snipes, and S. Ramaswami

Department of Mechanical Engineering, Clemson University, Clemson SC 29634, USA

* Correspondence: Email:gmica@clemson.edu; Tel: +1-864-656-5639; Fax: +1-864-656-4435.

Abstract: All-atom non-equilibrium molecular-dynamics simulations are used to investigate the problems of polyurea-borne tensile-stress waves interacting with a polyurea/fused-silica interface and fused-silica tensile-stress waves interacting with a fused-silica/polyurea interface, and the potential for the accompanying interfacial decohesion. To predict the outcome of the interactions of stress-waves with the material-interfaces in question, at the continuum level, previously determined material constitutive relations for polyurea and fused-silica are used within an acoustic-impedance-matching procedure. These continuum-level predictions pertain solely to the stress-wave/interface interaction aspects resulting in the formation of transmitted and reflected stress- or release-waves, but do not contain any information regarding potential interfacial decohesion. Present direct molecular-level simulations confirmed some of these continuum-level predictions, but also provided direct evidence of the nature and the extent of interfacial decohesion. In the molecular-level simulations, reactive force-field potentials are utilized to properly model the initial state of interfacial cohesion and its degradation during stress-wave-loading. Examination of the molecular-level interfacial structure before the stress-wave has interacted with the given interface, revealed local changes in the bonding structure, suggesting the formation of an "interphase." This interphase was subsequently found to greatly affect the polyurea/fused-silica decohesion strength and the likelihood for interfacial decohesion during the interaction of the stress-wave with the interface.

Keywords: polyurea; fused silica; interfacial decohesion; reactive force-fields

1. Introduction

1.1. Polyurea

The term *polyurea* refers to a class of elastomeric co-polymers which are synthesized via a fast reaction between difunctional isocyanate and difunctional amine precursors. A polyurea single chain consists of alternating hard segments and soft segments. As a result of strong hydrogen bonds and Π-electron interactions, hard segments of the adjacent chains (or of the same chain) are strongly attracted to each other, which promotes self-assembly/clustering. This causes bulk polyurea to typically be not homogeneous at the molecular level, but rather segregated, into discrete and dispersed *hard domains* and a continuous *soft matrix*. Since hard domains contain mostly a high glass transition temperature, T_g, hydrogen-bonded hard segments, they control polyurea strength and stiffness [1–6]. In contrast, since the soft matrix contains mostly low-T_g soft segments, it imparts high ductility to polyurea. The experimental and computational work carried out over the past decade [e.g. 7–12] has clearly established the ability of polyurea to: (a) increase the ballistic-penetration resistance of metallic and construction-material structures; and (b) disperse/attenuate the shockwaves resulting from blast and/or ballistic-impact loading.

In the present work, a clear distinction is made between (compressive) shockwaves and (tensile) stress-waves (investigated hereafter). With respect to its response to high-rate loading, polyurea (as well as fused-silica) can be characterized as an *acoustically normal* material, i.e. the wave speed increases with the extent of compression brought about by loading induced by propagating mechanical waves. Consequently, under compressive-loading conditions, a (discontinuous) shockwave is formed since trailing (higher compression) wavelets advance faster than their leading (lower compression) counterparts. Conversely, in the case of tensile loading, a continuous stress-wave with a progressively increasing front-width is formed since trailing (higher tension) wavelets advance slower than their leading (lower tension) counterparts. Although tensile-stress-waves can seriously damage protective structures, these waves have received relatively little attention compared to shockwaves (i.e. compressive-stress-waves) [e.g. 13–16].

1.2. Fused Silica

Despite the absence of a crystalline structure in glass (like fused silica), the microstructure of this material is not completely random. Rather, it involves different extents of short- and intermediate-range order spanning over a range of length-scales (from the quantum-mechanical to the continuum-level). To describe the structure of glass as determined using various experimental techniques, the so-called random network model [17] is typically employed. Such a model represents an amorphous material as a three-dimensional linked network of polyhedra. The character (number of facets) of the polyhedra is controlled by the species-specific coordination of the central (glass-forming) atom (cation). In the case of silicate-based glasses like fused silica, the polyhedron-center atoms are all silicon and each silicon atom is surrounded by four oxygen atoms (while each oxygen atom is connected to or bridges two silicon atoms), forming an SiO_4^{4-} tetrahedron. Since silicon has a tendency to form a continuous network with (bridging) oxygen atoms, SiO_2 (as well as boron and germanium oxides) is commonly referred to as a network former.

In addition to chemical modifications of ceramic-glass, changes in the microstructure of this material can be brought about by mechanical loading/deformation (typically requiring several GPa pressure levels). Specifically, high pressure may result in a reorganization of the atomic network (phase change) in the form of changes to the coordination of the network-forming cations. These phase changes can be of first order, which are characterized by the formation of a distinct high-pressure phase at a nominally constant pressure, or they may be of second order, which are phase changes which involve a continuous morphing of the original phase into the final high-pressure phase over a range of pressures. In the case of fused silica, second-order phase transformations were observed at pressures of 3 to 5 GPa, and involve relatively modest (3–7%) volume changes [18–21]. As far as the first-order phase transformations are concerned, they are observed at substantially higher pressures (ca. > 20 GPa), and are associated with substantially larger volume reductions and involve the formation of stishovite, an octahedrally-coordinated glass phase [18–21].

1.3. Reactive Force-field Potentials

In the all-atom molecular-level simulations carried out in the present work, constituent materials (polyurea and fused silica) are described using empirically-based particle/particle interaction (force-field potential) functions which capture the essential features of the valence-electron-based bonding without explicitly accounting for the presence of these electrons. Although, due to the empirical nature of their force-field functions, the all-atom molecular-level calculations are less accurate than their quantum-mechanical electronic-structure counterparts, they are associated with a number of advantages such as: (a) substantially reduced computational burden; (b) significantly larger computational domains analyzed (containing as many as tens or hundreds of millions of atoms, in comparison to several hundreds of atoms which could be handled using quantum-mechanical calculations); and (c) ability to analyze material behavior under large mechanical and/or thermal forces. In the case of (traditional) force-field potentials, quite different functional forms are used for different classes of materials (e.g. polymers, ceramics, metals, etc.). Consequently, interactions between adjoining materials with different types of bonding are typically either not accounted for, or accounted for inadequately. This is one of the main shortcomings of the traditional force-field potentials.

In the newly-developed reactive force-field potentials [e.g. 22], some of these shortcomings have been addressed. For example, within the reactive force-field potentials, interatomic bonding is not predetermined. Instead, bonding is taken to be the result of dynamic and adaptive interactions between the adjacent particles (i.e. atoms or ions). The reactive force-field potentials are based on two concepts: (a) particle self-consistent charge equilibration, which involves the atoms determining their own charges; and (b) inter-particle bond order (defined as the "theoretical index of the degree of bonding between two atoms relative to that of the bond provided by one localized electron pair" [23]). Akin to traditional force-fields, the reactive force-fields: (i) include environment-dependent multi-body interactions; and (ii) are generally parameterized using the pertinent quantum-mechanical and/or experimental data. The main improvements brought about by replacement of the traditional force-fields with reactive force-fields include [24]:

(a) the reactive force-fields enable reliable predictions of the material behavior not only in the states near equilibrium, but also further away from the equilibrium (e.g. in the product states

resulting from chemical reactions, which generally involve bond-breaking/-generation and atomic-charge changes); and

(b) analysis of the material behavior along the reaction paths, including the transition state, is enabled.

1.4. Main Objectives

The present work has the following three main objectives:

(a) Application of all-atom molecular-level non-equilibrium simulations involving reactive force-field potentials, for the purpose of obtaining the initial structure of the polyurea/fused-silica and fused-silica/polyurea material interfaces;

(b) Application of the same direct all-atom molecular-level simulations in conjunction with the stress-wave generation algorithm, in order to study the interaction of impinging tensile stress-waves onto these material interfaces; and

(c) Characterization of the nature and extent of interfacial decohesion as a function of the strength of the impinging tensile-stress-waves.

2. Reactive Force-field Function Formulation

The reactive force-field potential assumes that the total potential energy of the system contains a number of bond-order-dependent bonding and non-bonding components. Since the functional relationships for all the components of the reactive force-field potential can be found in a number of sources [e.g. 22], they will not be presented here. Because the reactive force-field parameters are generally assessed using large quantum-mechanics-based training datasets, they are transferable to new material systems containing the same chemical species as the systems used in the course of parameter-identification. In the present work, the parameterization of the reactive force-field potential for a system composed of carbon, hydrogen, oxygen, nitrogen and silicon given in [22] was used.

3. Molecular-Level Computational Analysis

All-atom molecular-level computational methods and tools are employed in the present work to investigate the interactions of polyurea-resident tensile stress-waves with a polyurea/fused-silica interface and fused-silica-resident tensile stress-waves with a fused-silica/polyurea interface. Within these methods and tools: (a) a material is considered as a system of interacting (and bonded) discrete particles (i.e. atoms, ions, etc.); and (b) potential-energy minimization-based (molecular statics) and Newton's second law-based (molecular dynamics) algorithms are employed to examine and quantify the behavior and properties of the material(s) under investigation. It is well-established that all-atom molecular-level computational methods and tools provide a good tradeoff between: (a) *ab initio* quantum mechanics methods, the methods which are intrinsically more accurate but limited to material systems containing no more than a few hundred interacting particles; and (b) meso-scale (also known as coarse-grained) computational methods, the methods which enable analysis of larger computational domains but rely on the concept of beads, larger hypothetical particles which account, in an approximate manner, for the collective behavior of the constituent atoms and ions.

Complete definition of an all-atom molecular-level computational model and analysis requires, in general, specification of: (a) geometrical (e.g. atomic positions, computational-cell size, etc.) and chemical (e.g. atomic species, bond order, etc.) details of the computational model and the associated particles; (b) a set of fully-parameterized force-field potential functions; and (c) details regarding the type, the number and the usage sequence of the molecular-level computational algorithms/methods to be used in the simulation. In addition to these three aspects of the computational model/analysis, the present work required introduction of a procedure for generation of planar longitudinal tensile stress-waves within the all-atom material molecular systems. The remainder of this section contains details regarding the aforementioned aspects of the present computational models and analyses, as well as specification of the problem analyzed in the present work.

3.1. All-Atom Molecular-Level Computational Models

As stated earlier, the primary objective of the present work is the analysis of polyurea-borne tensile stress-waves interacting with a polyurea/fused-silica interface and fused-silica tensile stress-waves interacting with a fused-silica/polyurea interface. In principle, such an analysis entails generation of a polyurea/fused-silica bi-material all-atom molecular-level model. However, as will be discussed later, such a model is incompatible with the use of the periodic boundary conditions, and with the procedure employed to generate tensile-stress waves. To remedy this problem, polyurea/fused-silica/polyurea and fused-silica/polyurea/fused-silica all-atom molecular-level models had to be generated. To generate such models, all-atom molecular models for pure polyurea and pure fused-silica subdomains are first generated and, then appropriately stacked in the direction of the stress-wave propagation.

3.1.1. Polyurea

During the construction of the computational model for polyurea, the procedure described in our prior work [13,14] was adopted. Towards that end, a rectangular parallelepiped-shaped computational unit-cell (extended in the direction of the propagating planar stress-waves) is constructed. Periodic boundary conditions are imposed across the cell faces in order to prevent spurious effects associated with the presence of free-surfaces. The three edges ($a = b < c$) of the cell are aligned respectively with the three global coordinate axes (x, y and z), with z being the stress-wave propagation direction. The procedure for construction of the pure polyurea all-atom molecular-level model developed in Refs. [13,14] involves the following steps: (a) construction of a single polyurea-chain repeat unit; (b) construction of a single polyurea chain; (c) construction of multiple polyurea chains and their inclusion into the computational cell; and (d) modification of the shape and position of the polyurea chains to obtain the necessary level of material nano-segregation in the initial state of polyurea. Visualizer program from Accelrys [25] was used for steps (a)–(b), Amorphous Cell program, also from Accelrys [26], was employed in step (c), while an in-house developed computer program was used to execute step (d). As Refs. [13,14] contain details of the all-atom molecular-level computational-model construction, these details will not be repeated here.

3.1.2. Fused-Silica

Akin to the polyurea case, the all-atom molecular-level computational model for fused-silica involves a rectangular parallelepiped-shaped computational cell. The cell is elongated in the direction of stress-wave propagation and subjected to the periodic boundary condition across its faces. As in the case of polyurea, the three edges ($a = b < c$) of the cell are aligned respectively with the three global coordinate axes. The following procedure, developed in our prior work [19,20], was employed in order to construct the computational cell for fused-silica:

(a) utilization of the Visualizer program [25] to construct a short silica-chain fragment;

(b) application of the Visualizer program in conjunction with a duplicate-and-attach process in order to grow the fragment generated in (a) and in turn to construct a fused-silica network structure; and

(c) employment of the Amorphous Cell program [26] in order to fill the computational cell with the fused-silica network, while ensuring that the target mass density of 2.200 g/cm^3 is reached.

3.1.3. Polyurea/Fused-Silica/Polyurea

Polyurea/fused-silica/polyurea sandwich structure all-atom molecular-level computational model was constructed by using two polyurea computational unit-cells (described in Section 3.1.1) to sandwich a single fused-silica unit-cell (described in Section 3.1.2) in the z-direction (the direction of stress-wave propagation). Towards that end it was ensured that the polyurea and the fused-silica unit-cells have identical edge lengths in the x-direction, as well as in the y-direction. A prototypical computational cell for polyurea/fused-silica/polyurea sandwich structure used in the present work is shown in Figure 1(a). Details regarding the all-atom molecular-level structure, including bonding, in the two interfacial regions of the polyurea/fused-silica/polyurea computational cells will be discussed in the later section.

3.1.4. Fused-Silica/Polyurea/Fused-Silica

Fused-silica/polyurea/fused-silica sandwich structure all-atom molecular-level computational model was constructed by using two fused-silica computational unit-cells (described in Section 3.1.2) to sandwich a single polyurea unit-cell (described in Section 3.1.1) in the z-direction (the direction of stress-wave propagation). This procedure required that the fused-silica and the polyurea unit-cells again have identical edge lengths in the x-direction, as well as in the y-direction. A prototypical computational cell for fused-silica/polyurea/fused-silica sandwich structure used in the present work is shown in Figure 1(b). Details regarding the all-atom molecular-level structure, including bonding, in the two interfacial regions of the fused-silica/polyurea/fused-silica computational cells will be discussed in the later section.

3.2. Reactive Force-field Parameter Identification

The two constituent materials contain the following chemical species: (a) polyurea - C, H, O and N; and (b) fused silica - Si, O. Thus, the interfacial regions contain the following species: C, H,

O, N and Si. The reactive force-field parameters for this five-component system have been taken from Ref. [27].

3.3. All-atom Molecular-level Computational Methods

All the calculations carried out in the present work employed two all-atom molecular-level computational methods: (a) molecular statics; and (b) molecular dynamics. The calculations are carried out using Discover, a molecular-level simulation program from Accelrys [28].
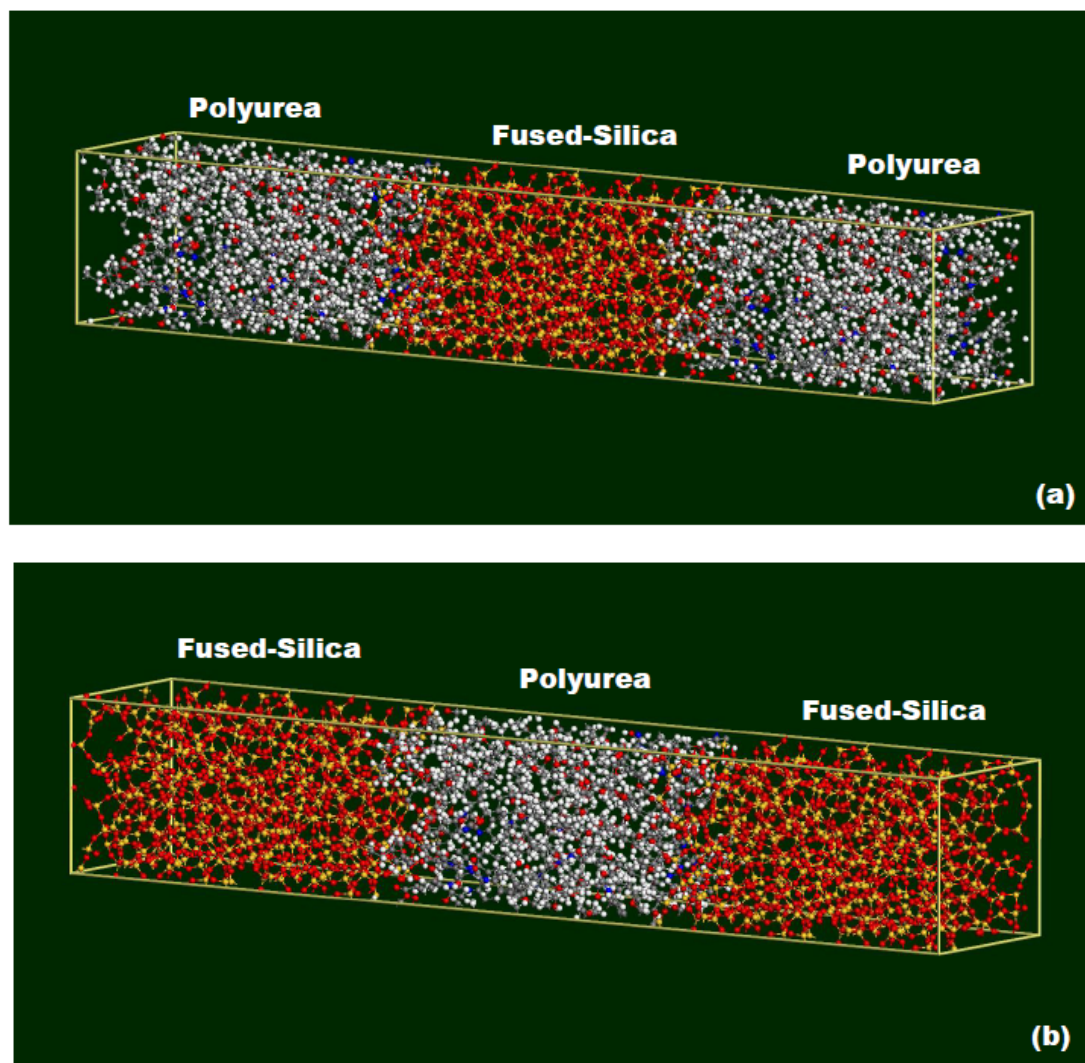
Figure 1. Computational cells for: (a) polyurea/fused-silica/polyurea; and (b) fused-silica/polyurea/fused-silica sandwich structures.

3.3.1. Molecular Statics

The molecular statics method can be described as a constrained-optimization technique. Within this method, the potential energy (objective function) of the computational cell (as defined by Eq. (1)) is minimized with respect to the positions of the constituent atoms/ions (design variables) subjected

to constraints related to the imposed periodic boundary conditions. Within Discover [28], the potential-energy minimization is conducted by adaptively and sequentially employing the Steepest Descent, Conjugate Gradient and Newton's minimization algorithms. Specifically, to reduce the computational cost, the Steepest Descent method is employed in the earliest stages of the minimization procedure, which allows a fast arrival at a molecular-level configuration which is quite close to its optimum counterpart (i.e. the one associated with the minimum potential energy). On the other hand, Newton's algorithm is employed in the latest stages of the minimization procedure, in order to ensure a monotonic and stable transition of the material into its optimal configuration.

In the present work, molecular statics is utilized to: (a) to minimize the potential energy of all four newly constructed all-atom molecular-level computational cells (described in Section 3.1); and (b) to help quantify the state of the material swept by a stress-wave, as will be discussed in greater detail in Section 4.

3.3.2. Molecular Dynamics

Within the molecular dynamics method, the associated Newton's equations of motion (three equations for each atom) are integrated numerically with respect to time in order to determine the temporal evolution of the material molecular-level configuration. Before such integration can be carried out, the forces acting on each atom/ion have to be determined. This was done by computing the negative gradient of the potential energy at the location of each atom, and setting it equal to the force experienced by that atom. Molecular dynamics methods are generally classified into equilibrium and non-equilibrium methods. Since both of these methods are employed in the present work, they are described in some detail in the remainder of this subsection.

Within the equilibrium molecular-dynamics methods, there is zero net flux of the mass, momentum and energy in each of the three principal coordinate directions. This is ensured by coupling the subject material system to the surroundings, such as a constant-pressure bath, a constant-temperature reservoir, etc., which also ensures that the system remains in a state of thermo-mechanical equilibrium, and the total mass within the computational cell remains constant. As will be discussed in greater detail in the next section, NVT (where N is the (fixed) number of atoms, V, the computational-cell volume (also fixed), and T (=298K) is the temperature) equilibrium molecular dynamics is employed in the first stage of the shock-generation procedure.

In the case of non-equilibrium molecular dynamics, the system is subjected to large mechanical and/or thermal perturbations (finite changes in the longitudinal, i.e. c, parameter of the computational cell, in the present case), resulting in large fluxes of mass, momentum and energy. Discover was initially designed to carry out only equilibrium molecular-dynamics simulations. To overcome this limitation, a procedure was devised to deactivate "equilibration" portions of this algorithm so that non-equilibrium molecular-dynamics calculations could be carried out.

3.4. Generation of All-atom Molecular-level Stress Waves

It should be recalled that by imposing periodic boundary conditions on the four computational cells described in Section 3.1, the resulting materials were made to be of an infinite extent. Consequently, molecular-level tensile-stress waves could be generated only in pairs (i.e. two stress-waves per computational cell). The molecular-level tensile-stress waves were generated in the

present work by employing a procedure which relies on a step-wise sequential expansion of the computational-cell longitudinal lattice parameter, c. This procedure involves the following steps: (a) a "sufficiently long" NVT molecular-dynamics simulation is conducted, before the stress-waves are generated, in order to thermally equilibrate the system at its target temperature (298 K); (b) to allow Discover to run in a non-equilibrium molecular-dynamics mode, the thermal-equilibration algorithm is disabled; (c) the tensile stress-waves are then initiated (and driven) by continuously moving the axial faces of the computational cell in opposite directions at a velocity u_p. This causes the longitudinal lattice-parameter c to increase as a function of time as:

$$c(t) = c(t = 0) + 2|u_p|t \qquad (1)$$

where t denotes time. As the two longitudinal faces of the computational cell are pulled apart, two converging tensile stress-waves are generated and driven in order to propagate the tensile stress, generated in the region adjacent to the longitudinal faces, to the remainder of the computational cell. In this way, (upstream) material particles swept by the waves acquire the velocity u_p, while the downstream particles remain unaffected by the approaching stress-waves. It should be noted that u_p for the z_{min} longitudinal face of the computational cell is negative, while that for the z_{max} longitudinal face is positive. In order to simulate the generation and propagation of tensile stress-waves of various strengths, $|u_p|$ is varied in a 200 to 1000 m/s range in the present work; and (d) in order to obtain planar, longitudinal (i.e. uniaxial-strain) stress conditions, computational-cell transverse lattice parameters a and b are kept constant during the application of the stress-wave-generation procedure.

The procedure for generating molecular-level tensile-stress waves described above results in the formation of two converging identical tensile-stress waves (at the computational-cell longitudinal faces), each moving towards the computational-cell center at a speed U_s of the given stress-wave wavelet. The concept of the stress-wave wavelet will be discussed in greater detail in Section 4. As these tensile stress-waves pass through the material, they cause an abrupt and substantial decrease in the material mass density, as well as abrupt and substantial increases in the internal-energy density, stress, and (absolute value of) particle velocity. In addition, interactions of these tensile-stress waves with the polyurea/fused-silica and fused-silica/polyurea material interfaces results in the formation of transmitted stress-waves and reflected stress-/release-waves, and may also result in interfacial decohesion.

A Discover input file [28] was used to carry out the procedure for generating molecular-level stress-waves, including the initial thermal-equilibration molecular-dynamics based procedure. This file is written using the Basic Tool Command Language (BTCL). This enabled the creation of a scripting engine that provides very precise control of simulation tasks, like sequential expansion of the computational cell in the longitudinal direction, deactivation of the thermal-equilibration algorithm during the stress-wave-generation process, etc.

3.5. Problem Formulation

The basic problem addressed in the present work was formulated as: (a) application of the modeling and analysis computational procedures described in the previous sections to construct molecular-level computational cells and the resident converging tensile-stress waves of various

strengths; (b) analysis of the material-configuration/dynamics results using a post-processing computational procedure, in order to determine the outcome of the interaction of the incident stress-waves with the material boundaries in question; and (c) a detailed characterization of the molecular-level microstructure of the interfacial regions prior to and following the incident-stress-wave/material-boundary interaction, in order to provide additional insight into the outcome of the stress-wave/interface mechanical interactions.

4. Results and Discussion

The major portion of this section deals with the presentation and discussion of the results pertaining to the interaction of tensile-stress waves with polyurea/fused-silica and fused-silica/polyurea interfaces. However, first a few important results obtained in the present work by extending our analysis introduced in Ref. [29] are presented and discussed. The latter results are found to be quite beneficial from the standpoint of predicting and rationalizing the outcome of the tensile-stress wave interaction with the material interfaces in question.

4.1. Relationships between Stress, Particle Velocity, Mass Density and Wave Speed

To obtain the basic functional relationships between the uniaxial-strain tensile stress, particle velocity, material mass density, and the speed of the wave-characteristics, the post-processing procedure based on the concept of so-called Lagrangian bins [29] was used in conjunction with the tensile-stress wave propagation results. These relationships for polyurea are given in Figures 2(a)–(d). The corresponding relationships for fused silica are given in Figures 3(a)–(d). It is seen that both polyurea and fused-silica behave as "normal" materials under tensile-loading conditions. That is, as the intensity of the tensile-stress wave is increased (as quantified by an increase in the tensile stress and the particle-velocity magnitude, and by a decrease in the material mass density), the associated stress-wave wavelet (a small portion of the stress-wave front) acquires a lower speed. Consequently, the tensile-stress wave front tends to spread (i.e. the leading-characteristic/trailing-characteristic distance increases) as the wave propagates through polyurea and fused-silica.

### 4.2. Application of the Impedance-Matching Procedure

The so-called impedance-matching procedure, which is used to predict the outcome of the interaction of the tensile stress-wave with the polyurea/fused-silica and fused-silica/polyurea material interfaces, is briefly overviewed in this section.

4.2.1. Polyurea-borne Tensile-Stress Wave Interaction with Polyurea/Fused-Silica Interface

Within the impedance-matching procedure, the functional relationships between the tensile stress, t_{11}, and the particle velocity, u_p, for the two materials in question are utilized. This type of relation is used because within the impedance-matching procedure, it is postulated that continuity of the stress and the particle velocities is maintained across the material boundary, during the interaction of a stress-wave with the material boundary, the interaction which results in the formation of a transmitted stress-wave and a reflected stress- or release-wave. In Figure 4(a), t_{11} vs. u_p relations for

polyurea and fused-silica are depicted (using solid lines) to help explain the impedance-matching method. Due to the fact that only the stress-wave propagating in the +z-direction (referred to hereafter as the right-propagating stress-wave) is analyzed, the particle velocities, shown in Figure 4(a) are negative. In addition, since the stress- waves are of a tensile nature, t_{11} takes on positive values. The states of the polyurea swept by one of the stress-wave wavelets and the stress-free quiescent fused-silica material, before the wavelet in question interacts with the polyurea/fused-silica interface, are denoted by a filled square (labeled A) and triangle (labeled B), respectively. After the interaction of the characteristic in question with the material interface, the state of the interfacial region is obtained by:

(i) mirroring the polyurea t_{11} vs. u_p curve about a vertical constant-u_p line (where u_p is associated with the stress-wave wavelet in question). The result of this exercise is depicted in Figure 4(a) using a dashed line; and
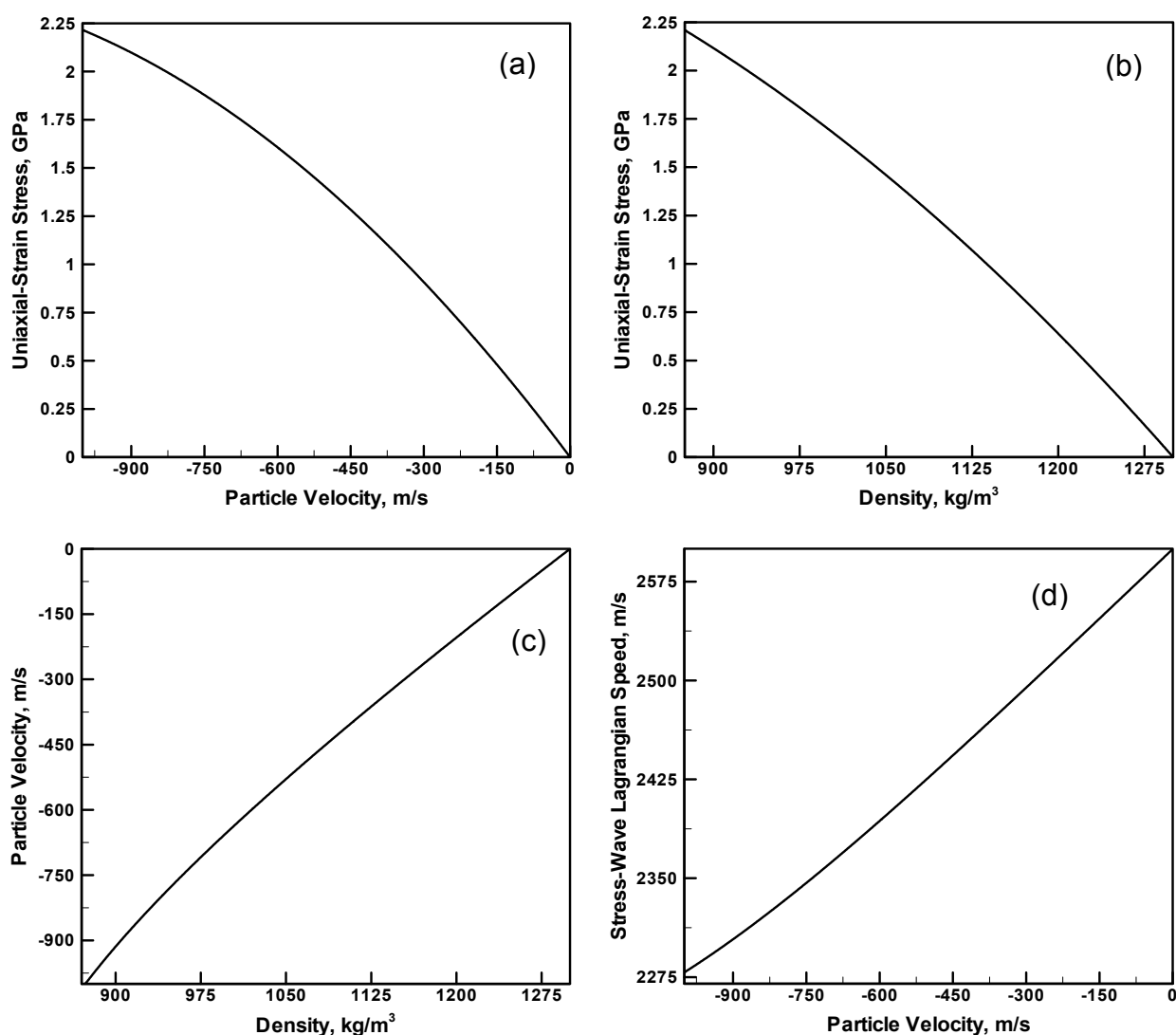
Figure 2. All-atom molecular-level computational-analysis-based relationships in polyurea: (a) longitudinal stress, t_{11}, vs. particle velocity, u_p; (b) t_{11} vs. material mass density, ρ; (c) u_p vs. ρ; and (d) stress-wave Lagrangian speed, U_W, vs. u_p.
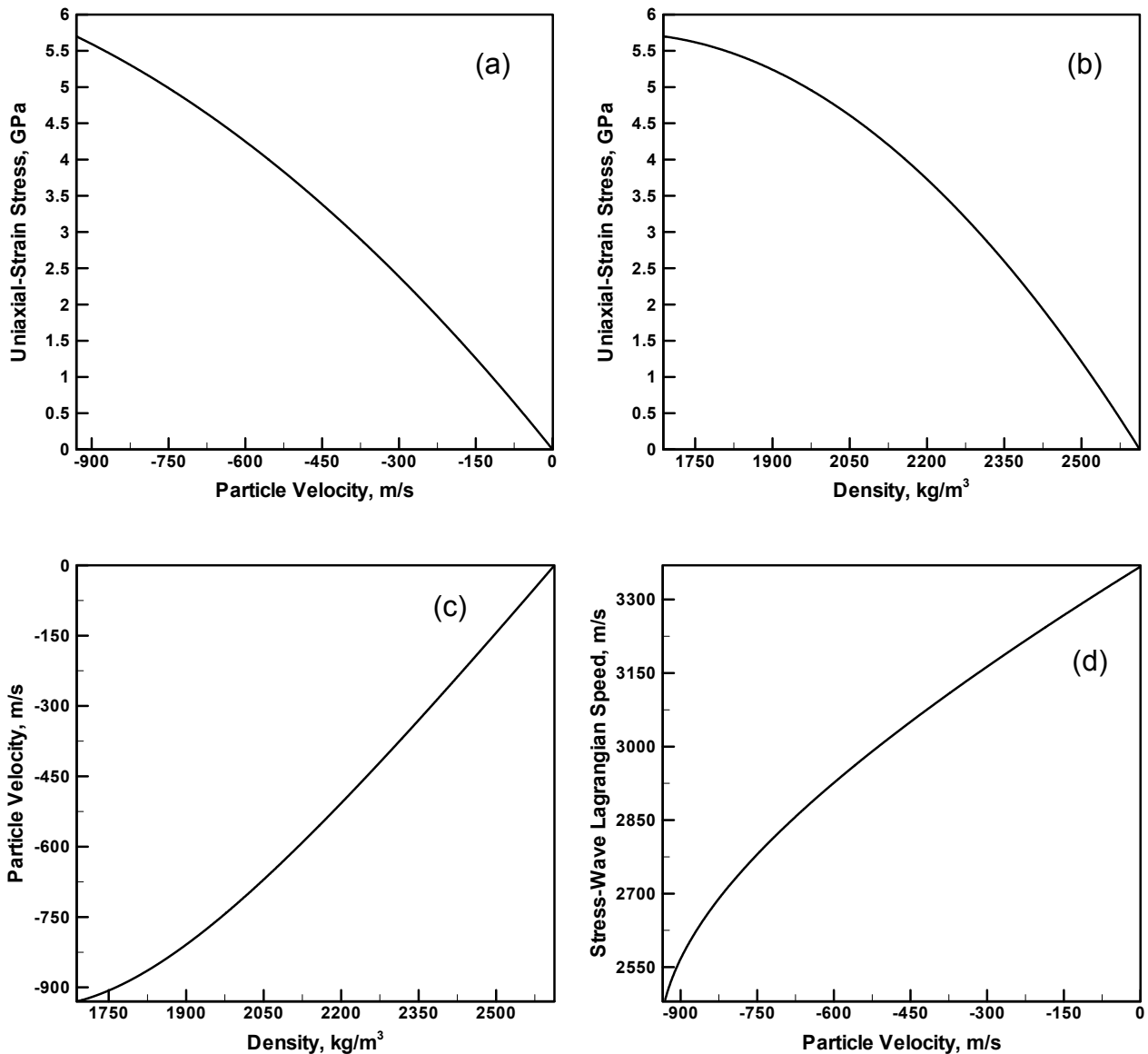
Figure 3. All-atom molecular-level computational-analysis-based Hugoniot-type relations in fused-silica: (a) longitudinal stress, t_{11}, vs. particle velocity, u_p; (b) t_{11} vs. material mass density, ρ; (c) u_p vs. ρ; and (d) stress-wave Lagrangian speed, U_w, vs. u_p.

(ii) the intersection of the mirrored polyurea curve with the fused-silica curve defines the states of the interfacial region after the interaction of the characteristic in question with the material interface, point C in Figure 4(a).

(a) Comparison of the polyurea and fused-silica states corresponding to point C with the material states corresponding to points A and B; (b) recognition of the fact that u_p is negative; and (c) the orientation of the polyurea and fused-silica t_{11} vs. u_p curves passing through point C reveal that: (i) a transmitted tensile wave is generated within fused-silica and, since the incident and the transmitted waves are of the same sense, the transmitted wave is also of a right-propagating character; and (ii) a reflected tensile-re-stress wave is generated within polyurea and, since the incident and the reflected waves are of opposite sense, the reflected wave is of a left-propagating character. It is the fact that the magnitude of t_{11} increases in the two materials as a result of the interaction of the right-

propagating incident stress-wave with the material boundary, that defines the tensile-stress/-re-stress character of the transmitted and reflected stress-waves. Also, since the polyurea is re-stressed by a left-propagating reflected wave, there is an accompanying decrease in the magnitude of the (negative) u_p.

Application of the impedance-matching procedure described above, and the results depicted in Figures 2(a)–(d) and 3(a)–(d), to the problem of interaction of an incident stress-wave within polyurea with the polyurea/fused-silica interface, is shown in Figures 5(a)–(f), the results labeled *Impedance-matching*. In Figure 5, parts (a), (c) and (e) correspond to the state of the polyurea/fused-silica bi- material before the incident-wave/material-interface interaction, while parts (b), (d) and (f) correspond to the state of the same bi-material after this interaction. Three state/kinematic variables are monitored in these figures: (i) particle velocity; (ii) stress; and (iii) mass density.

Examination of the results labeled *Impedance-matching* in Figures 5(a)–(f) reveals that the interaction of a right-propagating incident polyurea-resident stress-wave with the polyurea/fused-silica boundary: (i) creates a transmitted right-propagating stress-wave which imparts negative particle velocity and tensile stress to, while decreasing the mass density of, the "stressed" fused-silica; and (ii) creates a reflected left-propagating tensile-re-stress wave which decreases the magnitude of the particle velocity, increases the tensile stress and decreases the mass density of the swept polyurea. To help the reader visualize the direction of propagation of the incident, transmitted and reflected waves, arrows are used in Figures 5(a)–(f), as well as later in Figures 6(a)–(f).
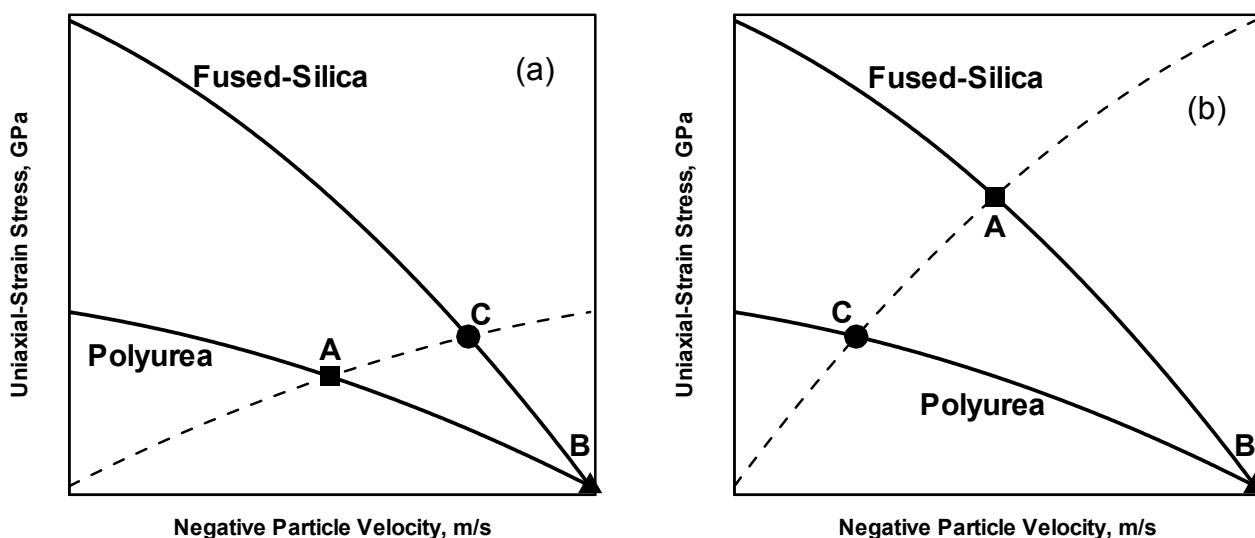
Figure 4. Impedance-matching procedure used to determine the outcome of the interaction of an incident stress-wave in: (a) polyurea with the polyurea/fused-silica interface; and (b) fused-silica with the fused-silica/polyurea interface. Please see text for explanation of the labeled points and dashed lines.
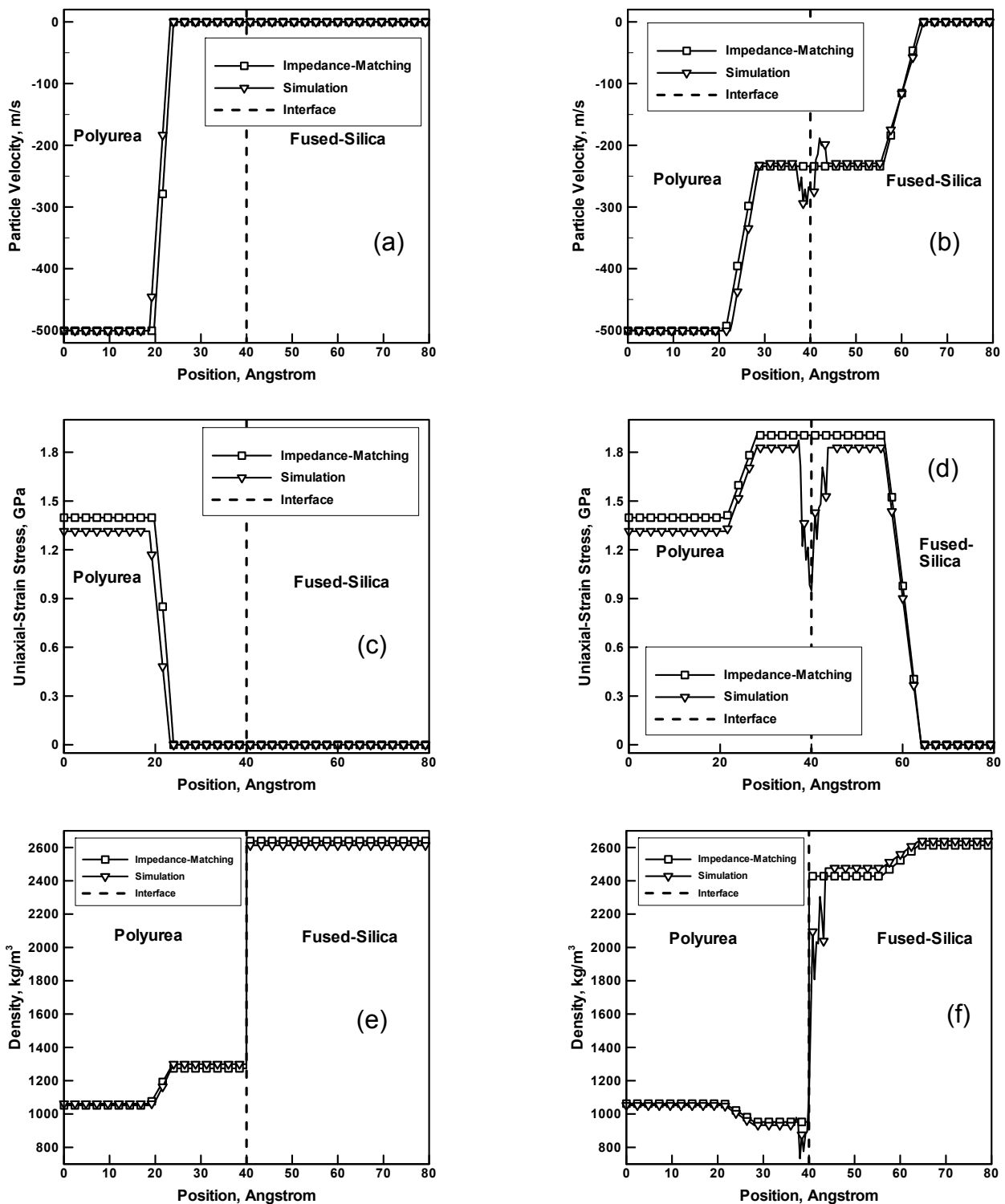
Figure 5. Distribution of the particle velocity, (a)–(b), axial stress, (c)–(d) and mass density, (e)–(f) along the length of the polyurea/fused-silica bi-material before, (a), (c), (e) and after, (b), (d), (f) the interaction of the incident stress-wave residing in polyurea with the polyurea/fused-silica boundary. Please see text for details.

4.2.2. Fused-Silica-borne Tensile-Stress Wave Interaction with Fused-Silica/Polyurea Interface

The impedance-matching procedure described in the previous subsection is also utilized in the case of the fused-silica-borne tensile-stress wave interacting with the fused-silica/polyurea interface. In this case, t_{11} vs. u_p relations for polyurea and fused-silica are depicted (using solid lines) in Figure 4(b). The states of the (stressed) fused-silica swept by one of the stress-wave wavelet and the stress-free quiescent polyurea material, before this right-propagating wavelet interacts with the fused-silica/polyurea interface, are denoted by a filled square (labeled A) and triangle (labeled B), respectively. Following the same impedance-matching procedure as that employed in the case of the polyurea-borne stress-wave, the state of the interfacial region after the interaction of the fused-silica-borne stress-wave with the fused-silica/polyurea interface is given by point C in Figure 4(b).

Using the same procedure as that in the case of polyurea-borne incident stress-waves reveals that: (i) a right-propagating transmitted tensile-stress wave is generated in the polyurea; and (ii) a left-propagating reflected compressive-release-wave is generated in the fused-silica. It is the fact that the magnitude of t_{11} decreases in the fused-silica as a result of the interaction of the incident stress-wave with the material boundary, that defines the release-wave character of the reflected wave. Also, since the pre-stressed fused-silica is relaxed by the passage of the release-wave, there is an accompanying increase in the (negative) u_p in this material.

Application of the impedance-matching procedure described above, to the problem of interaction of an incident stress-wave within fused-silica, with the fused-silica/polyurea interface, is shown in Figures 6(a)–(f). The results generated in these figures were obtained using the same procedure as that used in the generation of Figures 5(a)–(f).

Examination of the results labeled *Impedance-matching* in Figures 6(a)–(f) reveals that the interaction of an incident fused-silica-resident tensile-stress wave with the fused-silica/polyurea boundary: (i) creates a transmitted right-propagating stress-wave which imparts negative particle velocity and tensile stress to, while decreasing the mass density of, the *stressed* polyurea; and (ii) creates a left-propagating compressive-release wave which increases the magnitude of the particle velocity, decreases the tensile stress and increases the mass density of the swept fused-silica.

4.3. Molecular-Level Simulations of the Stress-Wave/Material-Interface Interactions

The all-atom simulation results pertaining to the interaction of a polyurea-borne stress-wave with polyurea/fused-silica interface and the interaction of a fused-silica-borne stress-wave with the fused-silica/polyurea interface are presented and discussed in this subsection. The results are analyzed in order to reveal spatial distribution and temporal evolution of the particle velocity, stress, and mass density prior to and after the stress-wave/material-boundary interaction.

4.3.1. Polyurea-borne Tensile-Stress Wave Interaction with Polyurea/Fused-Silica Interface

In contrast to subsection 4.2.1, in this subsection, the impedance-matching method was not used. Instead, the previously mentioned Lagrangian-bin method was combined with the virial theorem [30,31] and applied within a post-processing procedure to the all-atom-simulation results to determine the spatial distribution and temporal evolution of the particle velocity, stress, and mass

density prior to and after the stress-wave/material-boundary interaction. The results obtained using this procedure, labeled *Simulation*, are depicted in Figures 5(a)–(f).
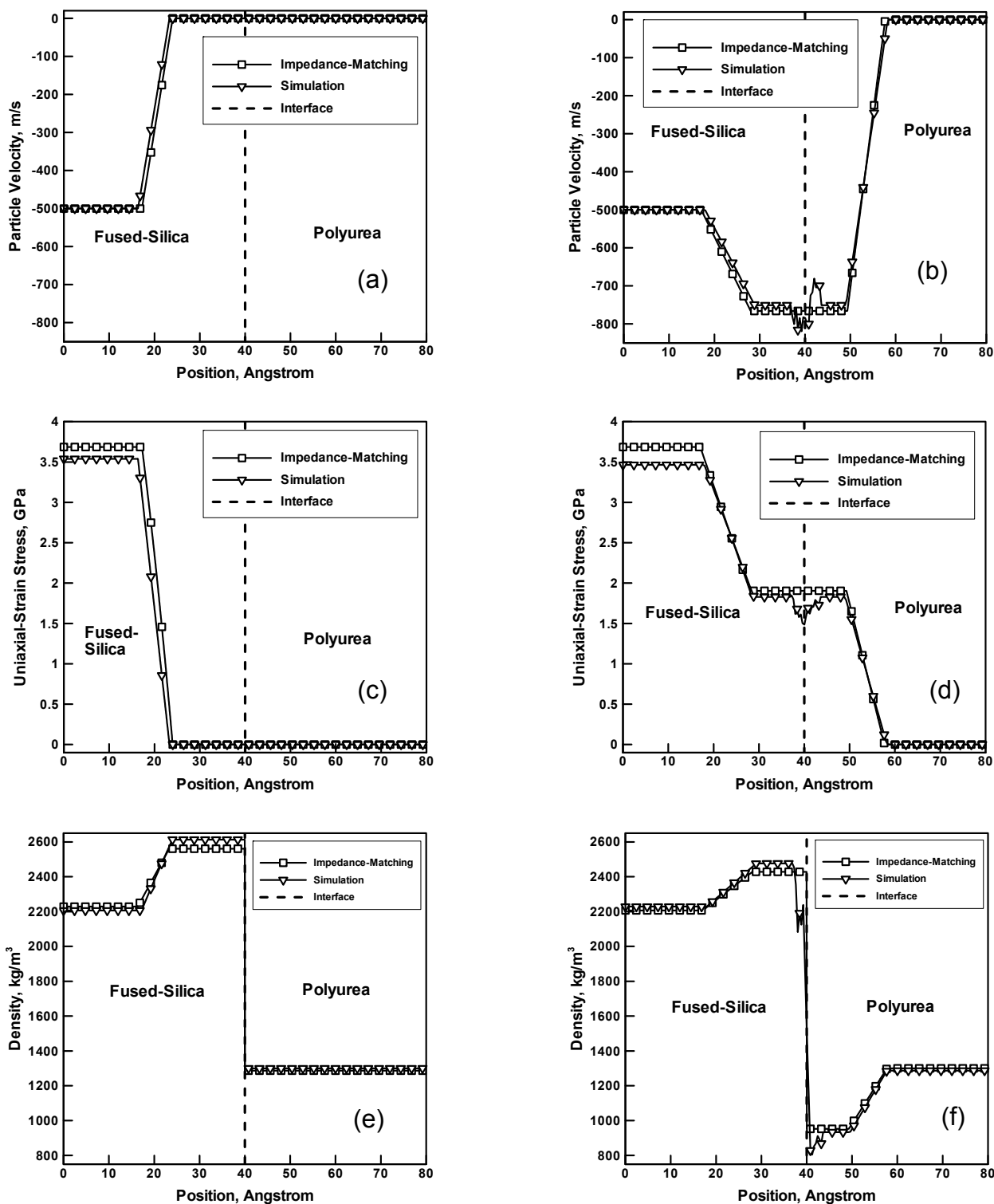
Figure 6. Distribution of the particle velocity, (a)–(b), axial stress, (c)–(d) and mass density, (e)–(f) along the length of the fused-silica/polyurea bi-material before, (a), (c), (e) and after, (b), (d), (f) the interaction of the incident stress-wave residing in fused-silica with the fused-silica/polyurea boundary. Please see text for details.

A comparison of the corresponding *Impedance-Matching* and *Simulation* results displayed in Figures 5(a)–(f) reveals:

(a) before the interaction of the incident polyurea-resident stress-wave with the polyurea/fused-silica interface, the location and shape of the stress-wave (as represented by the spatial distribution of the particle velocity, stress and mass density) are in fairly good agreement with their impedance-matching-based counterparts, Figures 5(a), (c) and (e); and

(b) as in the case of the *Impedance-Matching* results, the *Simulation* results show the formation of a transmitted right-propagating tensile-stress wave and a reflected left-propagating tensile-re-stress wave upon the interaction of the incident polyurea-resident tensile-stress wave with the polyurea/fused-silica interface, Figures 5(b), (d) and (f). However, the two sets of results considered show more differences than in the case of the incident stress-wave. Specifically, while continuity in the particle velocity and stress appears to be maintained in the case of the *Simulation-based* results, these results are quite irregular in the interfacial region. Further away from the interfacial region, the *Simulation* results tend to reacquire their "well-behaved" character. These findings suggest that, perhaps, the interaction of the incident stress-wave with the polyurea/fused-silica interface gives rise to some form of microstructural changes in the interfacial region.

4.3.2. Fused-Silica-borne Tensile-Stress Wave Interaction with Fused-Silica/Polyurea Interface

The results obtained in this portion of the work (labeled as *Simulation* in Figures 6(a)–(f)) are obtained using the same procedure as that employed in subsection 4.3.1. A comparison of the corresponding *Impedance-Matching* and *Simulation* results displayed in Figures 6(a)–(f) leads to similar findings as those made in the case of polyurea, Figures 5(a)–(f).

4.4. Stress-Wave Impact-Induced Changes in the Interfacial-Region Microstructure

In this subsection, the all-atom simulation results pertaining to the interaction of an incident polyurea-resident tensile-stress wave with a polyurea/fused-silica interface or the interaction of a fused-silica-resident tensile-stress wave with a fused-silica/polyurea interface are presented and discussed. The results are analyzed in order to reveal the changes experienced by the interfacial region after its interaction with the incident tensile-stress wave.

4.4.1. Polyurea-borne Tensile-Stress Wave Interaction with Polyurea/Fused-Silica Interface

The results presented in Section 4.3.1 suggested the possibility of microstructural changes in the polyurea/fused-silica interfacial region as a result of the tensile-stress wave interaction with the interface. In this section, the results obtained after the examination of the material microstructure in the polyurea/fused-silica interfacial region are presented and discussed. Figure 7(a) shows a relatively thin slice of the molecular structure of the polyurea/fused-silica bi-material prior to the arrival of the incident polyurea-resident stress-wave. Examination of this figure reveals the presence of a thin interfacial region within which bonding is established between the two adjoining materials. The same interfacial region following the interaction of the incident polyurea-resident stress-wave within the polyurea/fused-silica interface is depicted in Figure 7(b). Careful examination of the molecular structure displayed in this figure and its comparison with the results displayed in Figure

7(a) reveals that the interfacial region has undergone some microstructural changes as a result of its interaction with the incident stress-wave. Specifically, it is seen that some of the trans-interface bonds have been broken and that the two adjoining materials have undergone some decohesion/detachment. These microstructural changes can then be used to explain the aforementioned differences between the *Impedance-Matching* and *Simulation* results in the interfacial region, as observed in Figures 5(b), (d) and (f).
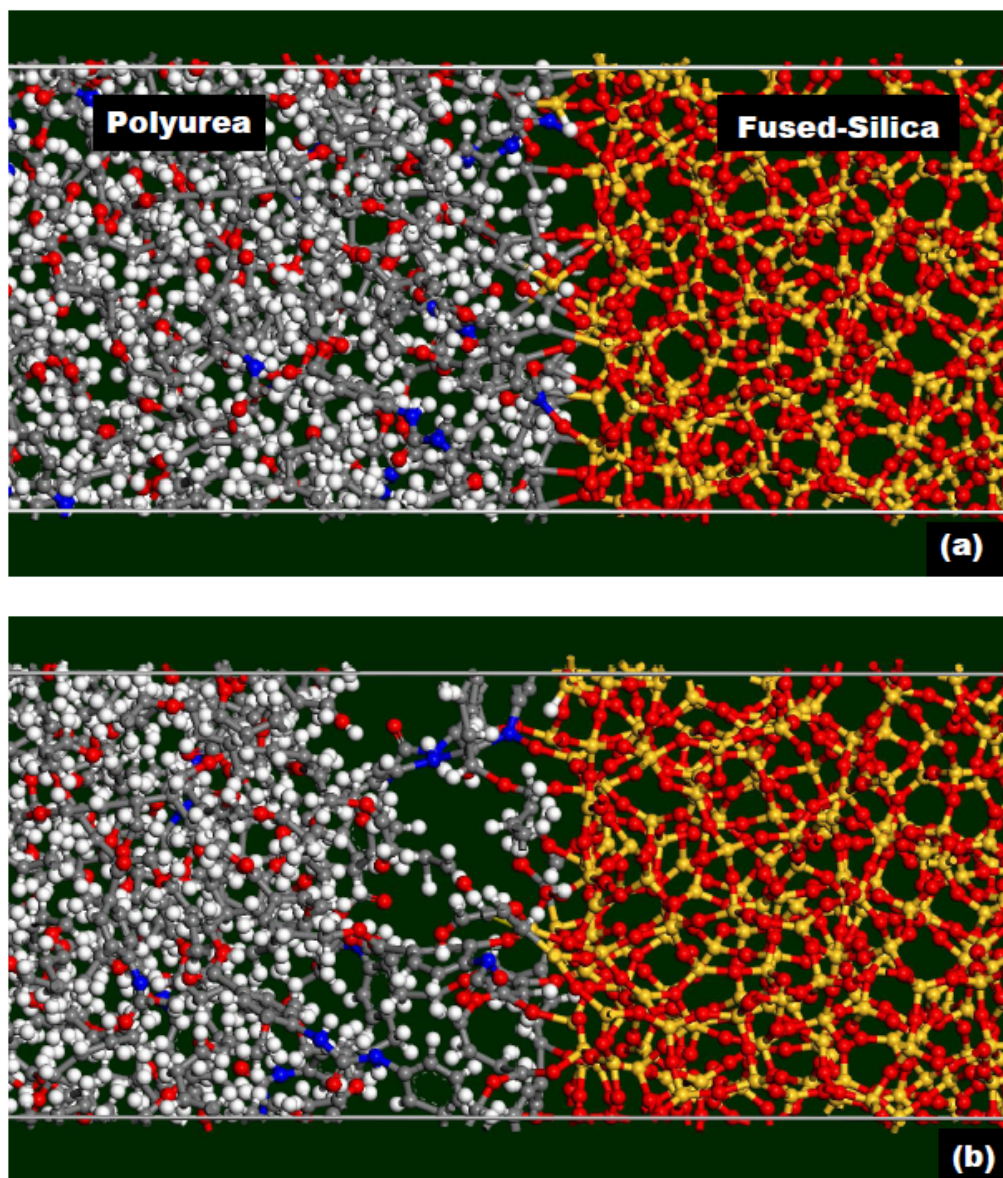
Figure 7. An example of the molecular-level microstructure in the polyurea/fused-silica bi-material: (a) before; and (b) after the arrival of the polyurea-resident right-propagating incident stress-wave to, and its interaction with, the polyurea/fused-silica interface.

4.4.2.   Fused-Silica-borne Tensile-Stress Wave Interaction with Fused-Silica/Polyurea Interface

Figure 8(a) shows a relatively thin slice of the molecular structure of the fused-silica/polyurea bi-material prior to the arrival of the incident fused-silica-resident tensile-stress wave. The same region as that shown in Figure 8(a) but after following the interaction of the incident fused-silica-resident stress-wave within the fused-silica/polyurea interface is depicted in Figure 8(b).
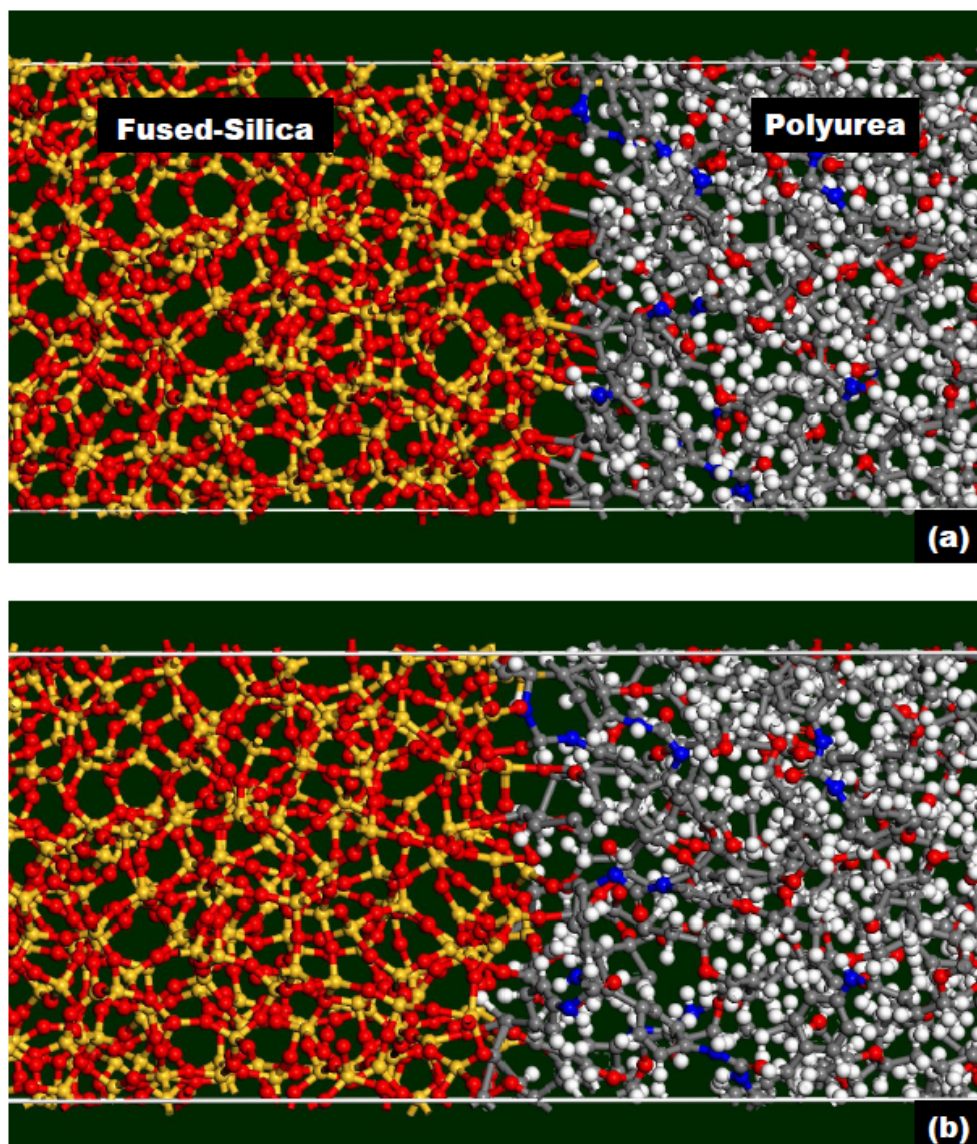
Figure 8. An example of the molecular-level microstructure in the fused-silica/polyurea bi-material: (a) before; and (b) after the arrival of the fused-silica-resident right-propagating incident stress-wave to, and its interaction with, the fused-silica/polyurea interface.

Examination of the results shown in Figures 8(a)–(b) leads to similar conclusions as those made in connection with Figures 7(a)–(b), respectively. The only significant difference is that the extent of the microstructural changes seen in Figure 8(b) is lower than that observed in the case of the

interaction of the incident polyurea-resident tensile-stress wave with the polyurea/fused-silica interface, Figure 7(b). This finding can be rationalized by the fact that while the intensity of the incident stress-waves (as measured by the peak-stress values) is identical in both stress-wave/interface interaction-cases, the reflected stress-wave in the case of Figure 7(b) is of a tensile-re-stress character (i.e. causes an increase in the interfacial tensile stress), while the reflected stress-wave in the case of Figure 8(b) is of a compressive-release character (i.e. causes a decrease in the interfacial tensile stress). In other words, the tensile stress experienced by the polyurea/fused-silica interface is larger than its counterpart in the fused-silica/polyurea case. Consequently, a larger extent of interfacial decohesion is expected and is observed in the former than in the latter case. It should be further noted that although the extent of microstructural changes is lower in the fused-silica/polyurea interface case, these changes are of a sufficiently large magnitude to affect spatial distribution and temporal evolution of the particle velocity, stress and mass density, Figures 6(b), (d) and (f).

5. Conclusion

Based on the results obtained in the present work, the following summary remarks and main conclusions can be drawn:

1. Interactions of polyurea-borne tensile stress-wave with polyurea/fused-silica interface and fused-silica-borne tensile stress wave with fused-silica/polyurea material interface are analyzed using all-atom molecular-level computational methods and tools.

2. The results related to the propagation of the stress-waves within polyurea and fused-silica (prior to the interaction with the corresponding material interface) are utilized to determine functional shock-Hugoniot-type relationships between the uniaxial-strain stress, particle velocity, mass density and the stress-wave speed.

3. The results obtained revealed that when the incident waves are sufficiently strong their interaction with respective material interface can give rise to microstructural changes involving interfacial bond-breaking and decohesion.

4. As a result of these microstructural changes, it is found that the characteristics of the transmitted stress-waves, as well as of the reflected stress-/release-waves are altered relative to their counterparts predicted by the well-known continuum type impedance-matching procedure. The latter procedure utilizes the Hugoniot-type relationships determined in the present work.

5. While no experimental results for the polyurea/fused-silica cohesion-strength are presently available, the computed cohesive-strength results obtained in the present work are found to be in the physically realistic range, and to be consistent with their experimental counterparts involving polyurea adjoined to another (non-fused-silica) material.

Conflict of Interest

All authors declare no conflicts of interest in this paper.

References

1. Grujicic M, Ramaswami S, Snipes JS, et al. (2014) Multi-scale computation-based design of nano-segregated polyurea for maximum shockwave-mitigation performance. *AIMS Mater Sci* 1: 15–27.
2. Grujicic M, Bell WC, Pandurangan B, et al. (2010) Blast-wave impact-mitigation capability of polyurea when used as helmet suspension pad material. *Mater Des* 31: 4050–4065.
3. Grujicic M, Snipes JS, Galgalikar R, et al. (2014) Material-model based determination of the shock-Hugoniot relations in nanosegregated polyurea. *J Mater Eng Perform* 23: 357–371.
4. Grujicic M, He T, Pandurangan B, et al. (2012) Experimental characterization and material-model development for microphase-segregated polyurea : an overview *J Mater Eng Perform* 21: 2–16.
5. Grujicic M, Pandurangan B, King AE, et al. (2011) Multi-length scale modeling and analysis of microstructure evolution and mechanical properties in polyurea. *J Mater Sci* 46: 1767–1779.
6. Castagna AM, Pangon A, Choi T, et al. (2012) The role of soft segment molecular weight on microphase separation and dynamics of bulk polymerized polyureas. *Macromol* 45: 8438–8444.
7. Bogoslovov RB, Roland CM, Gamache RM (2007) Impact-induced glass-transition in elastomeric coatings. *App Phys Let* 90: 221910.
8. Grujicic M, Pandurangan B, He T, et al. (2010) Computational investigation of impact energy absorption capability of polyurea coatings via deformation-induced glass transition. *Mater Sci Eng A* 527: 7741–7751.
9. Grujicic M, Bell WC, Pandurangan B, et al. (2011) Fluid/structure interaction computational investigation of the blast-wave mitigation efficacy of the advanced combat helmet. *J Mater Eng Perform* 20: 877–893.
10. Grujicic A, LaBerge M, Grujicic M, et al. (2012) Potential improvements in shockwave-mitigation efficacy of a polyurea-augmented advanced combat helmet: a computational investigation. *J Mater Eng Perform* 21: 1562–1579.
11. Grujicic M, d'Entremont BP, Pandurangan B, et al. (2012) Concept-level analysis and design of polyurea for enhanced blast-mitigation performance. *J Mater Eng Perform* 21: 2024–2037.
12. Grujicic M, d'Entremont BP, Pandurangan B, et al. (2012) A study of the blast-induced brain white-matter damage and the associated diffuse axonal injury. *Multidisc Model Mater Struc* 8: 213–245.
13. Grujicic M, Pandurangan B, Bell WC, et al. (2011) Molecular-level simulations of shockwave generation and propagation in polyurea. *Mater Sci Eng A* 528: 3799–3808.
14. Grujicic M, Yavari R, Snipes JS, et al. (2012) Molecular-Level computational investigation of shockwave mitigation capability of polyurea. *J Mater Sci* 47: 8197–8215.
15. Grujicic M, Snipes JS, Ramaswami S (2015) Meso-scale computational investigation of polyurea microstructure and its role in shockwave attenuation/dispersion. *AIMS Mater Sci* 2: 163–188.

16. Grujicic M, Snipes JS, Ramaswami S, et al. (2014) Meso-scale computational investigation of shock-wave attenuation by trailing release-wave in different grades of polyurea. *J Mater Eng Perform* 23: 49–64.

17. Kingery WD, Bowen HK, Uhlmann DR (1976) *Introduction to Ceramics*, 2nd Ed., New York: John Wiley & Sons, 91–124.

18. Grujicic M, Bell WC, Pandurangan B, et al. (2011) The effect of high-pressure densification on ballistic-penetration resistance of a soda-lime glass. *J Mater: Des and Appl* 225: 298–315.

19. Grujicic M, Bell WC, Glomski PS, et al. (2011) Multi-length scale modeling of high-pressure induced phase transformations in soda-lime glass. *J Mater Eng Perform* 20: 1144–1156.

20. Grujicic M, Bell WC, Pandurangan B, et al. (2012) Molecular-level simulations of shock generation and propagation in soda-lime glass. *J Mater Eng Perform* 21: 1580–1590.

21. Grujicic M, Pandurangan B, Zhang Z, et al. (2012) Molecular-level analysis of shock-wave physics and derivation of the Hugoniot relations for fused silica. *J Mater Eng Perform* 21: 823–836.

22. van Duin ACT, Dasgupta S, Lorant F, et al. (2001) ReaxFF: A reactive force field for hydrocarbons *J Phys Chem A* 105: 9396–9409.

23. IUPAC Gold Book, "bond order," http://goldbook.iupac.org/B00707.html, accessed November 22, 2013.

24. Chen H-P, Kalia RK, Kaxiras E, et al. (2010) Embrittlement of metal by solute segregation-induced amorphization. *Phys Rev Lett* 104: 155502.

25. Materials Visualizer Datasheet. Accelrys, Inc. (2014) Available from: http://accelrys.com/products/datasheets/materials-visualizer.pdf.

26. Amorphous Cell Datasheet. Accelrys, Inc. (2014) Available from: http://accelrys.com/products/datasheets/amorphous-cell.pdf.

27. Liu L, Liu Y, Zybin SV, et al. (2011) ReaxFF-lg: Correction of the ReaxFF reactive force field for London dispersion, with applications to the equations of state for energetic materials. *J Phys Chem A* 115: 11016–11022.

28. Discover Datasheet. Accelrys, Inc. (2014) Available from: http://accelrys.com/products/datasheets/discover.pdf.

29. Grujicic M, Yavari R, Snipes JS, et al. (2014) All-atom molecular-level computational simulations of planar longitudinal shockwave interactions with polyurea, soda-lime glass and polyurea/glass interfaces. *Multidisc Model Mater Struct* 10: 474–510.

30. Grujicic M, Ramaswami S, Snipes JS, et al. (2013) Axial-compressive behavior, including kink-band formation and propagation, of single p-phenylene terephthalamide (PPTA) fibers. *Adv Mater Sci Eng* 2013: Article ID 329549. doi: 10.1155/2013/329549.

31. Grujicic M, Yavari R, Snipes JS, et al. (2014) All-atom molecular-level computational analyses of polyurea/fused-silica interfacial decohesion caused by impinging tensile stress-waves. *Inter J Struc Integ* 5: 339–367.